arXiv:2509.09135v1 [cs.LG] 11 Sep 2025

Continuous-Time Value Iteration for Multi-Agent Reinforcement Learning

Xuefeng Wang*
School of Aeronautics and Astronautics
Purdue University
West Lafayette, IN 47907, USA
wang6067@purdue.edu

Lei Zhang*
Department of Computer Science
Purdue University
West Lafayette, IN 47907, USA
zhan5814@purdue.edu

Henglin Pu
School of Electrical and Computer Engineering
Purdue University
West Lafayette, IN 47907, USA
pu36@purdue.edu

Ahmed H. Qureshi†
Department of Computer Science
Purdue University
West Lafayette, IN 47907, USA
ahqureshi@purdue.edu

Husheng Li†
School of Electrical and Computer Engineering
& School of Aeronautics and Astronautics
Purdue University
West Lafayette, IN 47907, USA
husheng@purdue.edu

Abstract

Existing reinforcement learning (RL) methods struggle with complex dynamical systems that demand interactions at high frequencies or irregular time intervals. Continuous-time RL (CTRL) has emerged as a promising alternative by replacing discrete-time Bellman recursion with differential value functions defined as viscosity solutions of the Hamilton–Jacobi–Bellman (HJB) equation. While CTRL has shown promise, its applications have been largely limited to the single-agent domain. This limitation stems from two key challenges: (i) conventional solution methods for HJB equations suffer from the curse of dimensionality (CoD), making them intractable in high-dimensional systems; and (ii) even with HJB-based learning approaches, accurately approximating centralized value functions in multi-agent settings remains difficult, which in turn destabilizes policy training. In this paper, we propose a CT-MARL framework that uses physics-informed neural networks (PINNs) to approximate HJB-based value functions at scale. To ensure the value is consistent with its differential structure, we align value learning with value-gradient learning by introducing a Value Gradient Iteration (VGI) module that iteratively refines $\nabla_x V$ along trajectories. This improves gradient fidelity, in turn yielding more accurate values and stronger policy learning. We evaluate our method using continuous-time variants of standard benchmarks, including multi-agent particle environment (MPE) and multi-agent MuJoCo. Our results demonstrate that our approach consistently outperforms existing continuous-time RL baselines and scales to complex multi-agent dynamics.

*Equal contribution.
†Corresponding authors.

Preprint. Under review.

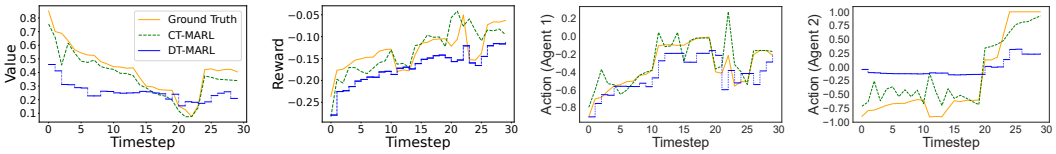

(a) Value Approximation (b) Reward Approximation (c) Agent 1 Action (d) Agent 2 Action

Figure 1: The performance of CT-MARL and DT-MARL is compared on a continuous-time, two-agent coupled oscillator task. DT-MARL suffers from significant bias and error when applied in the continuous domain. In contrast, CT-MARL yields smoother actions, higher rewards, and more accurate value approximations, closely aligning with the analytical LQR ground truth.

1 Introduction

RL has achieved remarkable success in a range of single- and multi-agent interaction tasks, including robotic manipulation [5], strategy games [39], wireless communications [12, 44] , and traffic coordination [16]. Most existing RL methods model these interactions in discrete time, where Bellman backup is computed at a fixed time interval. However, discrete-time RL (DTRL) is not well-suited for real-world scenarios that often demand high-frequency decision-making or operate at arbitrary, non-uniform time intervals (e.g., financial trading [33] and autonomous driving [21]). Specifically, DTRL methods tend to generalize poorly when deployed under time resolutions that differ from training, leading to suboptimal control and stability issues [41, 34]. To address these limitations, CTRL has emerged as an alternative to learn value functions in continuous time [9, 32]. However, existing works only focus on single-agent settings and have not yet been widely explored for multi-agent scenarios. In multi-agent domains, each agent must not only interact with the environment but also coordinate with other agents, all while coping with the chllenges like non-stationarity introduced by simultaneously learning policies. Within this context, our paper investigates a novel approach to solving CT-MARL problems. To better understand the limitations of DTRL and advantages of CTRL for multi-agent scenarios, we present a didactic case as shown in Fig. 1. In this simple continuous-time control task, DT-MARL fails to accurately approximate the true value functions, leading to incorrect control actions, particularly for agent 2. In contrast, our CT-MARL algorithm closely follows the ground-truth trajectory, maintains high returns, and generates accurate control actions for both agents.

Unlike Bellman operator-based DTRL [2], CTRL leverages HJB PDEs to compute differential value functions [27, 34]. However, solving HJB PDEs through conventional approaches (e.g., dynamic programming or discretization) suffers from CoD in high-dimensional dynamical systems [3], especially where the computational complexity grows exponentially with the state dimension in multi-agent systems. PINNs have emerged as a powerful tool to circumvent CoD [45], and offer convergence guarantees for problems with smooth solutions [35, 17]. To approximate the solutions of HJB PDEs, PINNs translate the underlying physics law (e.g., PDEs) along with boundary conditions into the loss functions to refine networks.

However, even with PINNs to alleviate the CoD in CT-MARL, learning accurate centralized value functions under the centralized training decentralized execution (CTDE) framework remains challenging. The inherent non-stationarity across agents makes value learning unstable [49], and standard PINNs, which rely solely on PDE and boundary residuals, often yield biased or noisy value gradients [51]. These inaccuracies propagate into the value function, undermining policy quality and stability. To address this limitation, we propose a novel learning approach that combines PINN and VGI information, which is used to optimize the value learning. The PINN component ensures the value approximations satisfy the HJB PDEs, while VGI iteratively propagates and refines the value gradient approximations along the sampled trajectories. This integration yields significantly more accurate value-gradient information, which enhances value approximation accuracy and ultimately improves policy learning.

Our work makes the following contributions. **(1)** We leverage PINNs to approximate differential value functions and apply them to solve *continuous-time multi-agent reinforcement learning* problems, which have rarely been explored by previous studies. **(2)** We introduce a novel *value-gradient iteration* term that dynamically refines the approximations of value gradients during training. This setting improves the computational accuracy of the value gradients, accelerates learning convergence, and leads to highly accurate value approximations, enabling efficient policy learning. **(3)** We

create continuous-time versions of two standard MARL benchmarks, the continuous-time MPE and continuous-time multi-agent MuJoCo. The results demonstrate that our method consistently surpasses other current CTRL baselines, highlighting the advantages of precise value-gradient learning in high-dimensional multi-agent systems.

2 Related Work

2.1 Continuous-Time Reinforcement Learning

CTRL has received increasing attention in recent years, however, most existing works focus on the single-agent settings [18, 23, 40, 47, 46, 38, 4, 11]. These studies aim to optimize policies in continuous-time domains, which avoids time discretization and achieves higher fidelity in control applications such as robotics and navigation. For instance, [4] proposes a continuous-time value iteration algorithm to solve the HJB equation without the need for a stabilizing initial policy. Similarly, [11] designs an actor-critic network for solving the infinite horizon HJB equations with theoretical guarantees. [23] designs two policy iteration algorithms that compute comprehensive solutions to HJB equations. In contrast, [18] introduces a temporal–difference learning based algorithm to deal with continuous-time problems via discretization. [47] develops a robust actor–critic framework for continuous-time nonlinear systems using unmodeled dynamics. [34] utilizes PINNs with ϵ-scheduling iteration to approximate the value function and empirically outperforms SOTA RL methods in continuous-time settings. [48] integrates neural ordinary differential equations (ODEs) to model uncertainty in state evolution using Bayesian inference, and further introduces a continuous-time actor-critic algorithm that circumvents challenges such as Q-function vanishment and poor discretization. CT-MARL remains relatively underexplored compared to the substantial studies for single-agent settings. [26] solves multi-agent pathfinding problem using fuzzy Q-learning, while [19] proposes a model-based value iteration algorithm tailored for continuous-time multi-agent systems. Beyond these examples, only a limited number of studies have addressed CT-MARL, which highlights the importance of our contributions.

2.2 Solving HJB Equations via PINNs

In single-agent optimal control or multi-agent cooperative settings, value functions are characterized as the viscosity solutions to HJB equations [7], which are the first-order nonlinear parabolic PDEs. However, solving HJB equations with conventional numerical methods is computationally intractable in high-dimensional settings due to CoD [30, 29]. Recent studies show that PINNs can mitigate CoD by leveraging their Monte Carlo nature when PDE solutions are smooth [45]. PINNs often approximate value functions using trainable neural networks by minimizing PDE-driven loss functions, including boundary residual [14, 15], PDE residual [1, 51], and supervised data derived from numerical solvers [28, 50]. Notably, recent studies demonstrate that integrating HJB-based PINNs with Proximal Policy Optimization (PPO) leads to improved performance over standard PPO in continuous-time single-agent MuJoCo environments [27]. However, solving CT-MARL problems through the integration of PINNs and RL remains an open and unexplored area of research.

3 Methodology

3.1 Problem Formulation

In this paper, we focus on multi-agent cooperative settings. Following the continuous-time control system framework [8, 48, 23], we formulate the continuous-time multi-agent problem as a tuple:

$$\mathcal{M} = \left\langle \mathcal{X}, \{\mathcal{U}_i\}_{i=1}^{N}, N, f, r, g, \{t_k\}_{k\geq 0}, T, \rho \right\rangle. \tag{1}$$

where $\mathcal{X} \subseteq \mathbb{R}^n$ is the state space and $\mathcal{U} = \mathcal{U}_1 \times \cdots \times \mathcal{U}_N \subseteq \mathbb{R}^m$ represents the joint action space of N agents. The global state and control input are represented by $x \in \mathcal{X}$ and $u \in \mathcal{U}$. Agent interactions occur over a fixed time horizon [0, T]. The multi-agent system evolves according to time-invariant nonlinear dynamics defined by $\dot{x} = f(x, u)$, where $f : \mathcal{X} \times \mathcal{U} \to \mathcal{X}$ is the global dynamics function. We define $\pi : \mathcal{X} \times [0, T] \to \mathcal{U}$ as the decentralized joint policy $\pi = (\pi_1, \ldots, \pi_N)$. All agents share a global reward $r : \mathcal{X} \times \mathcal{U} \to \mathbb{R}$ and a global terminal cost $g : \mathcal{X} \to \mathbb{R}$. $\rho \in (0, 1]$ is the discount factor or time-horizon scaling parameter. Unlike standard formulations that assume a

fixed time step, we consider a strictly increasing sequence of decision times $\{t_k\}_{k\geq 0}$ with variable gaps $\tau_k = t_{k+1} - t_k > 0$. In this paper, we assume that $\mathcal{U}_i$ is compact and convex; f is Lipschitz continuous; r and g is Lipschitz continuous and bounded.

Definition 1 (Value Function of Multi-agent Systems)**.** Given $u = (u_1, \ldots, u_N)$ as a joint control input, the optimal global value function is defined as:

$$V(x) = \max_{u\in\mathcal{U}} \int_t^\infty e^{-\rho(\tau-t)} r(x(\tau), u(\tau) d\tau \tag{2}$$

3.2 HJB and Policy Learning

For CT-MARL problems, we adopt the HJB theory to solve continuous-time problems. In this subsection, we explain how the HJB equation is leveraged to solve the CT-MARL problems. Specifically, we define a value network V_θ parametrized by a set of weights and biases θ, and describe *how the global value function V_θ is trained* and *how each agent's policy π_{ϕ_i} is updated*, such that the overall procedure serves as a continuous-time analogue of actor–critic policy iteration.

3.2.1 Critic Learning with HJB.

First, we present the following Lemma to show that the optimal value function $V(x,t)$, as defined in Eq. (2), is the optimal solution to HJB PDEs [7] in the context of cooperative multi-agent settings.

Lemma 3.1 (HJB for Multi-agent Systems)**.** For all $(x,t) \in \mathcal{X} \times [0,T]$, the value function $V(x,t)$ is the optimal solution to satisfy the HJB PDEs and boundary conditions:

$$-\rho V(x,t) + \partial_t V(x,t) + \nabla_x V(x,t)^\top f\big(x,u^*\big) + r\big(x,u^*\big) = 0, \tag{3}$$

where optimal control input $u^* = \arg\max_{u\in\mathcal{U}} \mathcal{H}(x,t,\nabla_x V(x,t))$, and boundary condition is $V(x,T) = g(x)$. The Hamiltonian $\mathcal{H}$ is defined as $\mathcal{H} = \nabla_x V(x,t)^\top f\big(x,u\big) + r\big(x,u\big)$.

The proof is attached in Appendix A.1.

To approximate differential value functions, we aim to solve the HJ PDEs given in Eq. (3). However, solving such PDEs through numerical methods becomes computationally intractable for problems with state dimensions higher than 6 [6]. To address this challenge, we adopt PINNs, which approximate value functions to satisfy both PDE residuals and boundary conditions. Specifically, we define HJB PDE residual as

$$\mathcal{R}_\theta(x,t) = -\rho V_\theta(x,t) + \partial_t V_\theta(x,t) + \nabla_x V_\theta(x,t)^\top f(x,u) + r(x,u). \tag{4}$$

and minimize both residual loss and boundary condition loss towards zero during model refinement.

$$\mathcal{L}_{\text{res}} = \big\|\mathcal{R}_\theta(x,t)\big\|_1, \quad \mathcal{L}_{\text{term}} = \big\|V_\theta(x,T) - g(x)\big\|_2^2. \tag{5}$$

3.2.2 Policy Learning

While analytical optimal control laws can be derived in some cases by maximizing the Hamiltonian, such closed-form solutions might not be available in complex multi-agent systems such as MPE or MuJoCo. To overcome this challenge, we use an actor network to generate control inputs, replacing the need for analytical controls in the critic network used to approximate value functions. The actor and critic networks are refined iteratively until convergence, enabling the actor network to approximate optimal control policies. During training, we compute a continuous-time advantage function derived by residual $\mathcal{R}_\theta(x,t)$. This advantage function is used for policy gradient, where each agent's decentralized policy $\pi_{\phi_i}(u_i \mid x,t)$ is optimized to maximize long-term return.

Lemma 3.2 (Instantaneous Advantage)**.** Assume the one-step Q-function over a short interval $\delta t > 0$ be

$$Q(x,t,u) = r(x,u)\,\delta t + e^{-\rho\delta t} V\big(x(t+\delta t), t+\delta t\big). \tag{6}$$

Then the instantaneous advantage satisfies

$$A(x,t,u) = -\rho V(x,t) + \partial V_t(x,t) + \nabla_x V(x,t)^\top\, f(x,u) + r(x,u). \tag{7}$$

The proof is attached at Appendix A.2.

With the critic's instantaneous advantage:

$$A_\theta(x,t,u) = -\rho V_\theta(x,t) + \partial_t V_\theta(x,t) + \nabla_x V_\theta(x,t)^\top f(x,u) + r(x,u), \tag{8}$$

we update each agent's policy network $\pi_{\phi_i}(u_i \mid x,t)$ in a decentralized fashion. For agent i, we minimize the negative expected advantage under the joint policy:

$$\mathcal{L}_{p_i} = -A_\theta\big(x,t,u\big)\log \pi_{\phi_i}\big(u_i \mid x,t\big), \tag{9}$$

Here, $u = (u_i, u_{-i})$ denotes the joint action, where $u_i \sim \pi_{\phi_i}$ is sampled from agent i's policy, and u_{-i} represents the actions of all other agents, sampled as $u_{-i} \sim \pi_{\phi_{-i}}$.

Lemma 3.3 (Policy Improvement)**.** Let π_{old} be the current joint policy and π_{new} the updated policy after one gradient step on the actor loss $\mathcal{L}_p$ with sufficiently small step size. Then:

$$Q^{\pi_{\text{new}}}(x,t,u) \geq Q^{\pi_{\text{old}}}(x,t,u). \tag{10}$$

The proof can be found at Appendix A.3.

3.3 Value Gradient Iteration Module

The performance of continuous-time control policies depends critically on the accuracy of the value, which in turn depends not only on the precision of its own approximation but also on the correctness of the value gradient $\nabla_x V(x,t)$. Recent studies have demonstrated that the accuracy of the value directly affects the computational closed-form control inputs [51, 27, 10]. However, the gradients obtained from standard PINN training are often noisy or misaligned with true trajectory behavior. Although prior work [51] improves value gradient approximations using supervised data, such ground-truth gradients are often inaccessible or prohibitively expensive to compute in complex, high-dimensional multi-agent settings. To address this, we introduce the VGI module that iteratively refines the value gradient approximations during training.

Definition 2 (VGI Gradient Estimator)**.** Given a small time step Δt, the VGI estimator of the value gradient at (x_t, u_t) is defined by

$$\nabla_x V(x_t,t) = \nabla_x r(x_t,u_t)\Delta t + e^{-\rho\Delta t}\nabla_x f(x_t,u_t)^\top \nabla_x V(x_{t+\Delta t}, t+\Delta t). \tag{11}$$

The VGI target in Eq. (11) can be interpreted as a one-step unrolling of the Bellman equation in the space of gradients. The first term captures the instantaneous contribution of the local reward gradient, while the second term propagates the downstream value information through the Jacobian of the system dynamics. This construction resembles a semi-discretized version of the value gradient flow and provides a practical surrogate for supervised gradient learning in the absence of ground-truth derivatives. The derivation process is posted at Appendix A.4.

Theorem 3.4 (Convergence of VGI)**.** Let $G : \mathbb{R}^d \to \mathbb{R}^d$ be defined as

$$G(\zeta) = \nabla_x r(x_t,u_t)\Delta t + e^{-\rho\Delta t}\nabla_x f(x_t,u_t)^\top \zeta, \tag{12}$$

and assume the dynamics $\|\nabla_x f(x_t,u_t)\|$ is bounded . Then G is a contraction, and the sequence $\zeta^{(k+1)} = G(\zeta^{(k)})$ converges to a unique fixed point $\zeta^* \in \mathbb{R}^d$.

The proof is detailed at Appendix A.5

Rather than introducing a separate network to predict value gradients, we directly compute the automatic derivative of the shared PINN critic $V_\theta(x,t)$. This gradient is then trained to match the VGI-generated target defined in Eq. (11). Specifically, we minimize the mean squared error between the computed and target gradients:

$$\mathcal{L}_{\text{vgi}} = \big\|\nabla_x V_\theta(x_t,t) - \hat{g}_t\big\|_2^2, \tag{13}$$

where $\hat{g}_t = \nabla_x r_\phi(x_t,u_t,\Delta t)\Delta t + e^{-\rho\Delta t}\nabla_x f_\psi(x_t,u_t,\Delta t)^\top \nabla_x V_\theta(x_{t+\Delta t}, t+\Delta t)$. Here, $r_\phi(x,u,\Delta t)$ denotes a reward models and $f_\psi(x,u,\Delta t)$ represents a dynamics model, where ϕ and ψ are respective network parameters.

3.4 Implementation Details

While the previous sections introduced our continuous-time actor–critic framework and the VGI module for value-gradient consistency, several practical considerations are essential to make the overall method operational and effective.

3.4.1 Dynamics Model and Reward Model

In a continuous-time setting, the true dynamics are given by $\dot{x} = f(x, u)$, but directly learning f via $\frac{x_{t+\Delta t} - x_t}{\Delta t}$ as a supervision target is pretty unstable in practice. Instead, we adopt a discrete-time model-based approach [36, 20, 13] that we train a neural network $f_\psi(x_t, u_t, \Delta t)$ to predict the next state $x_{t+\Delta t}$ via

$$\mathcal{L}_{\text{dyn}} = \left\| f_\psi(x_t, u_t, \Delta t) - x_{t+\Delta t} \right\|_2^2. \tag{14}$$

After learning f_ψ, we recover the continuous-time derivative by finite differences $\frac{f_\psi(x_t, u_t, \Delta t) - x_t}{\Delta t}$.

Similarly, we fit a reward network $r_\phi(x_t, u_t, \Delta t)$ to the observed instantaneous reward r_t:

$$\mathcal{L}_{\text{rew}} = \left\| r_\phi(x_t, u_t, \Delta t) - r_t \right\|_2^2. \tag{15}$$

Both f_ψ and r_ϕ are trained jointly, enabling us to compute the VGI module's target.

3.4.2 Anchor Loss for Critic Network

In addition to the HJB residual and terminal-condition losses, we incorporate a TD-style anchor loss to improve both the stability and accuracy of value learning. While the residual loss enforces the correctness of the value gradient, it does not constrain the value of $V(x, t)$. Terminal-condition losses can provide such supervision, but they often rely on access to well-defined terminal targets, which may be unavailable in complex continuous control environments such as MuJoCo. In these cases, the anchor loss offers an additional source of value landscape, helping the critic produce reasonable value approximations even when terminal rewards are sparse, delayed, or difficult to specify. We define the one-step return as:

$$R_t = r(x_t, u_t)\Delta t + e^{-\rho \Delta t} V_\theta\big(x_{t+\Delta t},\, t + \Delta t\big). \tag{16}$$

The anchor loss then enforces the value network to match these returns:

$$\mathcal{L}_{\text{anchor}} = \left\| V_\theta(x_t, t) - R_t \right\|_2^2. \tag{17}$$

The overall critic objective combines all four losses:

$$\mathcal{L}_{\text{total}} = \underbrace{\mathcal{L}_{\text{res}}}_{\text{HJB residual}} + \underbrace{\lambda_{\text{term}}\, \mathcal{L}_{\text{term}}}_{\text{terminal BC}} + \underbrace{\lambda_{\text{anchor}}\, \mathcal{L}_{\text{anchor}}}_{\text{TD anchor}} + \underbrace{\lambda_g\, \mathcal{L}_{\text{vgi}}}_{\text{VGI consistency}} . \tag{18}$$

Here $\lambda_{\text{term}}, \lambda_{\text{anchor}}, \lambda_g$ are tunable weights balancing PDE fidelity, terminal supervision, value-bootstrap anchoring, and gradient consistency. In practice, we jointly train the reward model, dynamics model, and value network using the data from the current trajectory. The detailed training process is listed in Appendix A.6.

4 Experimental Results

We evaluate our **Value Iteration via PINN (VIP)** method on two continuous-time multi-agent benchmarks: MPE [25] and multi-agent MuJoCo [37, 31]. In addition, we design a didactic benchmark, coupled oscillator (see details in Appendix B.1), to analyze value gradient approximations. This case study is easy to follow and enables the numerical computation of true values and their gradients, which provides a clear and interpretable setting to validate the effectiveness of VIP. Our experiments are designed to answer the following four key questions: **(1)** *Overall efficacy:* Does the proposed VIP model outperforms existing continuous-time RL baselines in these environments? **(2)** *VGI ablation:* How much does the VGI module contribute to final performance and training stability? **(3)** *PINN design choice:* How does activation function choice and loss term weighting in critic network affect the performance of VIP? **(4)** *Time discretization impact:* How well do discrete-time and continuous-time methods perform under arbitrary or unfixed time intervals?

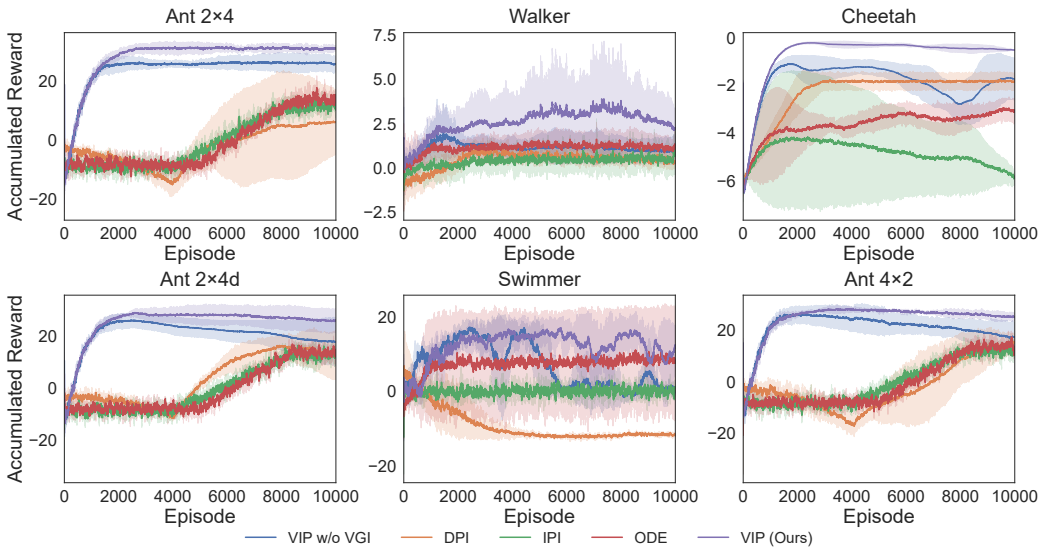

Figure 2: Performance across continuous-time multi-agent MuJoCo settings. The y-axis shows the mean cumulative reward.

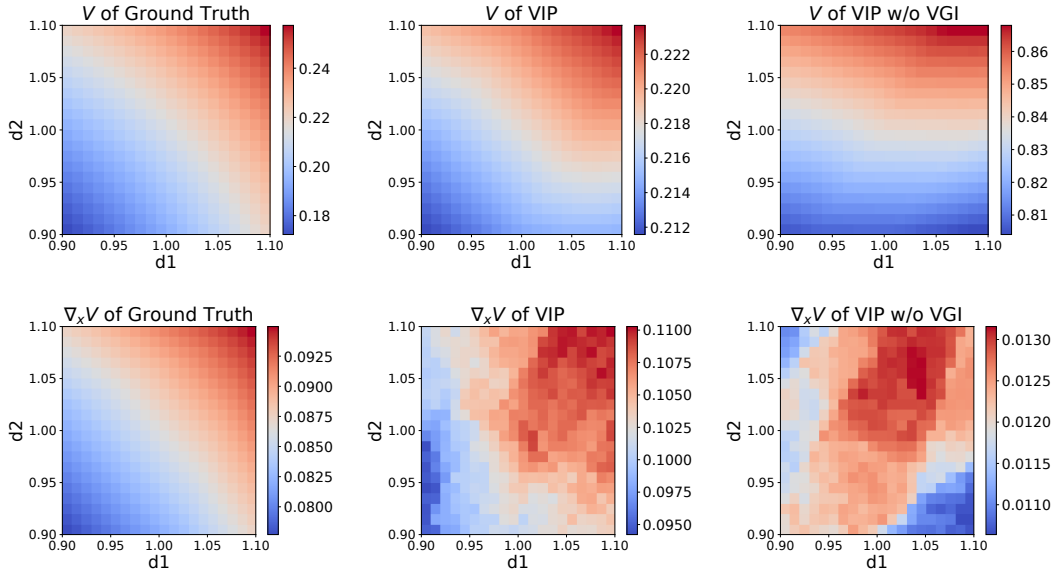

Figure 3: V and $\nabla_x V$ contour using VIP w/ VGI and w/o VGI in d_1-d_2 frame.

Benchmarks. We evaluate our method against baselines across eight experimental settings. We extend the MPE framework to a continuous-time formulation by using a variable-step Euler integration scheme, where the time interval Δt is sampled from a predefined range at each step. Experiments are conducted on the cooperative `navigation` and `predator prey` environments. Similarly, we adapt MuJoCo to continuous-time settings and evaluate on a suite of multi-agent locomotion tasks, including `ant` (2×4, 2×4d, 4×2), `walker`, `swimmer`, and `cheetah`. Further implementation details of these benchmarks are provided in Appendix B.2 and B.3. Lastly, we introduce a simple yet illustrative `coupled oscillator` environment to highlight the behavior of exact value functions, value gradients, and the relative performance of different methods under a controlled setting.

4.1 Baseline Methods

To evaluate our CT-MARL framework VIP, we compare against three continuous-time policy iteration baselines and include an ablated variant of our method without VGI: **CT-MBRL (ODE)** [48]: A continuous-time model-based RL approach that learns sys-

tem dynamics via Bayesian neural ODEs. This method uses an actor-critic framework to approximate state-value functions and derive the continuous-time optimal policies. **Differential Policy Iteration (DPI)** [23]: A model-based method with differential policy iterations that alternates between (i) solving the HJB PDEs to approximate continuous-time value functions and (ii) updating the policy by following the instantaneous gradient of value approximations.

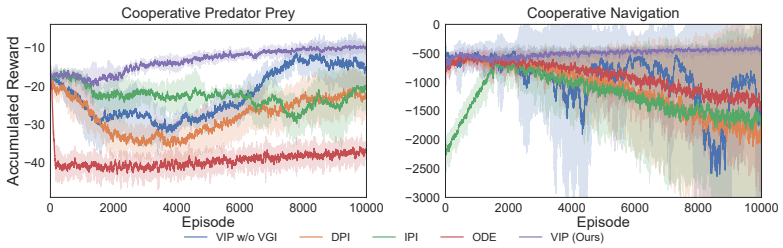

Figure 4: Performance across continuous-time MPE settings. The y-axis shows the mean cumulative reward.

Integral Policy Iteration (IPI) [23]: A partially model-free approach with integral policy iterations that reformulates the value function as a continuous integral, avoiding explicit differentiation during policy improvement. In our experimental settings, we discretize the integral, roll out trajectories to accumulate rewards, and fit a policy to minimize the resultant value functions. **Ablation (w/o VGI)**: An ablated version of VIP without VGI, which isolates the efficacy of value gradient refinement.

4.2 Results Analysis

Model Performance. We evaluate all RL methods in MPE and MuJoCo environments using five random seeds and report the mean cumulative reward curves in Fig. 2 and 4. The results show that VIP with VGI consistently converges fastest and achieves the highest final return across all tasks, which empirically validates the efficacy of integrating PINNs with RL. As HJB equations are PDEs with a single boundary condition at terminal time, PINN may struggle to backpropagate the correct physics information when relying solely on boundary values, often resulting in poor value approximations [22, 51]. To address this limitation, we incorporate the anchor and VGI loss terms in

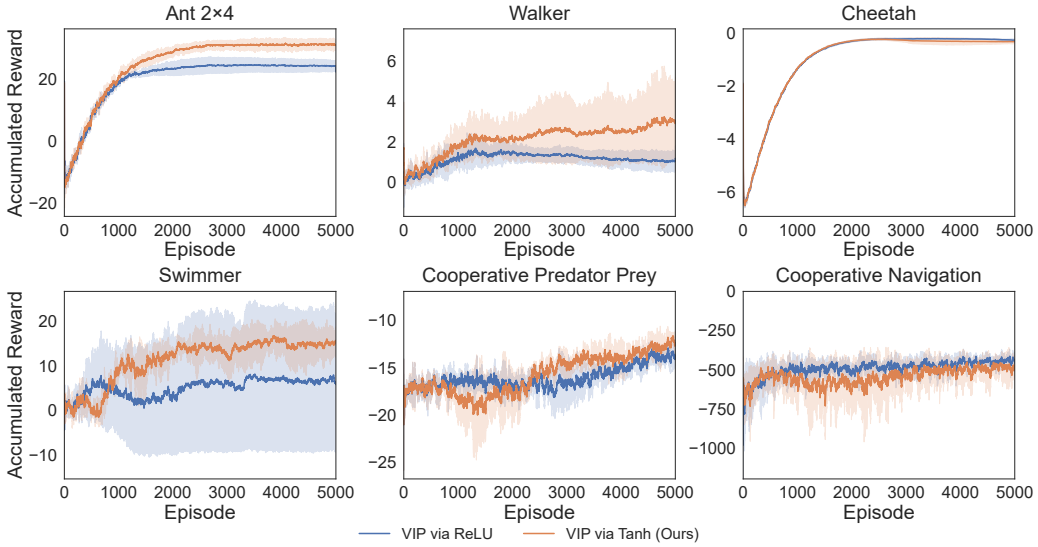

Figure 5: VIP performance with ReLU and Tanh activation functions in MuJoCo and MPE settings.

Eq. (18), which capture the landscape of value and its gradient so that PINNs converge to the true values. Ablation results further confirm the importance of VGI: removing VGI leads to significantly lower cumulative rewards across all experiments. This observation is consistent with the conclusion in the previous studies [50], which further strengthens that accurate value gradient approximation is crucial for effective PINN training and policy improvement.

To further demonstrate the importance of VGI, we revisit the didactic example, generate 400 rollouts from sampled initial states, and compute the average value using models with and without VGI. As shown in Fig. 3, the value contour projected onto the d_1–d_2 frame reveals that the model with VGI

closely matches the ground truth in both structure and scale, while the model without VGI produces significantly biased approximations. These results confirm that adding VGI is necessary to improve the accuracy of value approximations. A detailed comparison of the corresponding value gradients is also illustrated in Fig. 3. Furthermore, we evaluate the sensitivity of each loss term for the critic network by measuring the minimum distance to prey in Fig. 6, which highlights the critical role of PINN in refining value and policy networks.

Choice of PINN Design. We first examine the impact of activation function choice when incorporating PINN-based losses into critic network refinement. Specifically, we train VIP using ReLU and Tanh activations in both MuJoCo and MPE environments and report the accumulated rewards in Fig. 5. The results show that the VIP with Tanh consistently achieves higher accumulated rewards than the one with ReLU across all tasks. This experiment indicates the importance of activation function choice when using PINN-based losses to refine the critic network and has a consistent conclusion with the previous studies [1, 51]. The good performance of Tanh can be attributed to its smoothness and differentiability, which are particularly important when using PINNs to solve PDEs. PINNs typically use fully-connected network architectures and rely on auto-differentiation to compute value gradients for PDEs. The PINN residuals, including PDEs and boundary conditions, are further optimized using gradient descent. Smooth activation functions like Tanh support stable and accurate gradient flow throughout training, enabling more effective value approximations. In contrast, VIP with ReLU often encounters zero-gradient regions during backpropagation, which results in gradient explosion for deeper network architectures or degrades the learning of value functions due to insufficient nonlinearity. Therefore, the choice of a smooth activation function like Tanh is better suited for physics-informed learning, thereby ensuring more accurate approximations of the value functions.

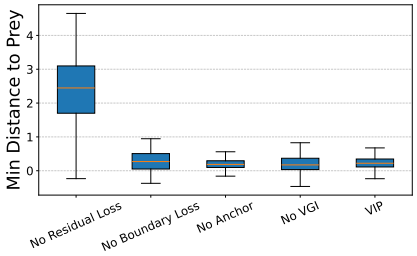

Figure 6: Ablation study of different loss terms in critic network for cooperative predator prey.

We also investigate the impact of weight parameters for PINN loss terms during VIP training. Specifically, we evaluate three configurations in Eq. (18): 1) balanced weights for all loss terms; 2) a large weight for boundary condition while keeping the others balanced; 3) a large weight for HJB residual with balanced weights for the remaining terms. As shown in Fig. 7, the best accumulated reward performance is achieved when all loss terms are properly balanced. Imbalanced weight settings yield stiffness in the training dynamics of PINNs [42], which makes the dominant loss term (with the largest weights) converge faster than the others [43]. In our experiments, such an imbalance causes VIP only to satisfy the PDEs or boundary conditions during training, ultimately leading to poor value approximations. Lastly, we evaluate the robustness of VIP and MADDPG [24] by generating rollouts with varying time intervals in the didactic environment and computing the average return across these rollouts. Fig. 8 illustrates that VIP maintains a nearly constant return across different time intervals, whereas MADDPG's performance degrades significantly as the interval increases. This result highlights the advantage of VIP in continuous-time multi-agent scenarios.

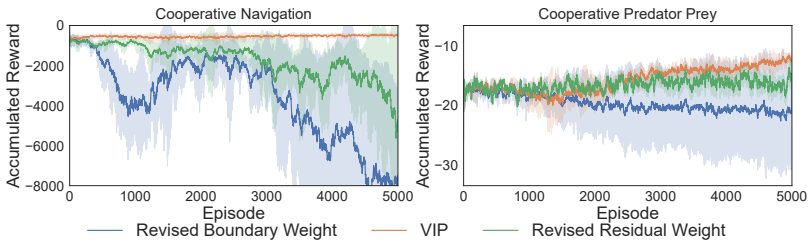

Figure 7: VIP performance with different weight settings in critic losses.

5 Conclusion and Limitations

We propose a novel approach that integrates PINNs into the actor-critic framework to solve CT-MARL problems. Specifically, we approximate value functions using HJB-based PINNs and introduce VGI to improve value approximations, thus mitigating the adverse impact of inaccurate value approximations on policy learning. We validate our VIP across continuous-time variants of MPE and MuJoCo environments and empirically demonstrate that VIP converges faster and achieves higher accumulated reward compared to baselines of SOTA. Furthermore, we investigate the importance of activation function choice and loss term weighting for VIP performance. In summary, our proposed VIP offers a promising approach to solve CT-MARL problems. However, we notice the limitation of VIP: the current work only focuses on cooperative CT-MARL tasks. Many real-world multi-agent scenarios involve competitive interactions, which have not yet been explored within CT-MARL frameworks. In competitive settings, agents no longer share a common value function, and such values often become discontinuous due to collision penalties in the reward function, which poses convergence challenges for PINN [51]. As part of future work, we aim to extend VIP to explore competitive CT-MARL problems, particularly those involving state constraints.

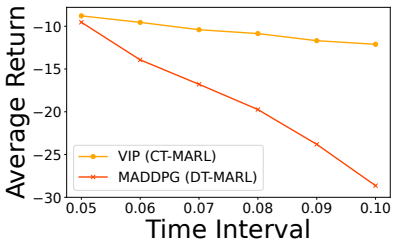

Figure 8: CT-MARL and DT-MARL performance under different time intervals.

References

[1] Somil Bansal and Claire J Tomlin. DeepReach: A deep learning approach to high-dimensional reachability. In *2021 IEEE International Conference on Robotics and Automation (ICRA)*, pages 1817–1824. IEEE, 2021.

[2] Richard Bellman. Dynamic programming. *science*, 153(3731):34–37, 1966.

[3] Richard Bellman, Robert E Kalaba, et al. *Dynamic programming and modern control theory*, volume 81. Citeseer, 1965.

[4] Tao Bian and Zhong-Ping Jiang. Reinforcement learning and adaptive optimal control for continuous-time nonlinear systems: A value iteration approach. *IEEE transactions on neural networks and learning systems*, 33(7):2781–2790, 2021.

[5] Lukas Brunke, Melissa Greeff, Adam W Hall, Zhaocong Yuan, Siqi Zhou, Jacopo Panerati, and Angela P Schoellig. Safe learning in robotics: From learning-based control to safe reinforcement learning. *Annual Review of Control, Robotics, and Autonomous Systems*, 5(1):411–444, 2022.

[6] Minh Bui, George Giovanis, Mo Chen, and Arrvindh Shriraman. Optimizeddp: An efficient, user-friendly library for optimal control and dynamic programming. *arXiv preprint arXiv:2204.05520*, 2022.

[7] Michael G Crandall and Pierre-Louis Lions. Viscosity solutions of Hamilton-Jacobi equations. *Transactions of the American mathematical society*, 277(1):1–42, 1983.

[8] Kenji Doya. Reinforcement learning in continuous time and space. *Neural computation*, 12(1): 219–245, 2000.

[9] Kenji Doya. Reinforcement learning in continuous time and space. *Neural computation*, 12(1): 219–245, 2000.

[10] Onno Eberhard, Claire Vernade, and Michael Muehlebach. A pontryagin perspective on reinforcement learning. *arXiv preprint arXiv:2405.18100*, 2024.

[11] Mohamad Kazem Shirani Faradonbeh and Mohamad Sadegh Shirani Faradonbeh. Online reinforcement learning in stochastic continuous-time systems. In *The Thirty Sixth Annual Conference on Learning Theory*, pages 612–656. PMLR, 2023.

[12] Amal Feriani and Ekram Hossain. Single and multi-agent deep reinforcement learning for ai-enabled wireless networks: A tutorial. *IEEE Communications Surveys & Tutorials*, 23(2): 1226–1252, 2021.

[13] Danijar Hafner, Timothy Lillicrap, Ian Fischer, Ruben Villegas, David Ha, Honglak Lee, and James Davidson. Learning latent dynamics for planning from pixels. In *International conference on machine learning*, pages 2555–2565. PMLR, 2019.

[14] Jiequn Han and Jihao Long. Convergence of the deep bsde method for coupled fbsdes. *Probability, Uncertainty and Quantitative Risk*, 5(1):1–33, 2020.

[15] Jiequn Han, Arnulf Jentzen, and Weinan E. Solving high-dimensional partial differential equations using deep learning. *Proceedings of the National Academy of Sciences*, 115(34): 8505–8510, 2018.

[16] Ammar Haydari and Yasin Yılmaz. Deep reinforcement learning for intelligent transportation systems: A survey. *IEEE Transactions on Intelligent Transportation Systems*, 23(1):11–32, 2020.

[17] Kazufumi Ito, Christoph Reisinger, and Yufei Zhang. A neural network-based policy iteration algorithm with global h 2-superlinear convergence for stochastic games on domains. *Foundations of Computational Mathematics*, 21(2):331–374, 2021.

[18] Yanwei Jia and Xun Yu Zhou. Policy evaluation and temporal-difference learning in continuous time and space: A martingale approach. *Journal of Machine Learning Research*, 23(154):1–55, 2022.

[19] Yi Jiang, Weinan Gao, Jin Wu, Tianyou Chai, and Frank L Lewis. Reinforcement learning and cooperative h∞ output regulation of linear continuous-time multi-agent systems. *Automatica*, 148:110768, 2023.

[20] Lukasz Kaiser, Mohammad Babaeizadeh, Piotr Milos, Blazej Osinski, Roy H Campbell, Konrad Czechowski, Dumitru Erhan, Chelsea Finn, Piotr Kozakowski, Sergey Levine, et al. Model-based reinforcement learning for atari. *arXiv preprint arXiv:1903.00374*, 2019.

[21] B Ravi Kiran, Ibrahim Sobh, Victor Talpaert, Patrick Mannion, Ahmad A Al Sallab, Senthil Yogamani, and Patrick Pérez. Deep reinforcement learning for autonomous driving: A survey. *IEEE transactions on intelligent transportation systems*, 23(6):4909–4926, 2021.

[22] Aditi Krishnapriyan, Amir Gholami, Shandian Zhe, Robert Kirby, and Michael W Mahoney. Characterizing possible failure modes in physics-informed neural networks. *Advances in neural information processing systems*, 34:26548–26560, 2021.

[23] Jaeyoung Lee and Richard S Sutton. Policy iterations for reinforcement learning problems in continuous time and space—fundamental theory and methods. *Automatica*, 126:109421, 2021.

[24] Ryan Lowe, Yi I Wu, Aviv Tamar, Jean Harb, OpenAI Pieter Abbeel, and Igor Mordatch. Multi-agent actor-critic for mixed cooperative-competitive environments. *Advances in neural information processing systems*, 30, 2017.

[25] Ryan Lowe, Yi I Wu, Aviv Tamar, Jean Harb, OpenAI Pieter Abbeel, and Igor Mordatch. Multi-agent actor-critic for mixed cooperative-competitive environments. *Advances in neural information processing systems*, 30, 2017.

[26] David Luviano and Wen Yu. Continuous-time path planning for multi-agents with fuzzy reinforcement learning. *Journal of Intelligent & Fuzzy Systems*, 33(1):491–501, 2017.

[27] Amartya Mukherjee and Jun Liu. Bridging physics-informed neural networks with reinforcement learning: Hamilton-jacobi-bellman proximal policy optimization (hjbppo). *arXiv preprint arXiv:2302.00237*, 2023.

[28] Tenavi Nakamura-Zimmerer, Qi Gong, and Wei Kang. Adaptive deep learning for high-dimensional Hamilton–Jacobi–Bellman equations. *SIAM Journal on Scientific Computing*, 43 (2):A1221–A1247, 2021.

[29] Stanley Osher and Chi-Wang Shu. High-order essentially nonoscillatory schemes for Hamilton–Jacobi equations. *SIAM Journal on numerical analysis*, 28(4):907–922, 1991.

[30] Stanley Osher, Ronald Fedkiw, and K Piechor. Level set methods and dynamic implicit surfaces. *Appl. Mech. Rev.*, 57(3):B15–B15, 2004.

[31] Bei Peng, Tabish Rashid, Christian Schroeder de Witt, Pierre-Alexandre Kamienny, Philip Torr, Wendelin Böhmer, and Shimon Whiteson. Facmac: Factored multi-agent centralised policy gradients. *Advances in Neural Information Processing Systems*, 34:12208–12221, 2021.

[32] Yulia Rubanova, Ricky TQ Chen, and David K Duvenaud. Latent ordinary differential equations for irregularly-sampled time series. *Advances in neural information processing systems*, 32, 2019.

[33] Ali Shavandi and Majid Khedmati. A multi-agent deep reinforcement learning framework for algorithmic trading in financial markets. *Expert Systems with Applications*, 208:118124, 2022.

[34] Alena Shilova, Thomas Delliaux, Philippe Preux, and Bruno Raffin. *Learning HJB Viscosity Solutions with PINNs for Continuous-Time Reinforcement Learning*. PhD thesis, Inria Lille-Nord Europe, CRIStAL-Centre de Recherche en Informatique, Signal . . . , 2024.

[35] Yeonjong Shin, Jerome Darbon, and George Em Karniadakis. On the convergence of physics informed neural networks for linear second-order elliptic and parabolic type pdes. *arXiv preprint arXiv:2004.01806*, 2020.

[36] Richard S Sutton. Dyna, an integrated architecture for learning, planning, and reacting. *ACM Sigart Bulletin*, 2(4):160–163, 1991.

[37] Emanuel Todorov, Tom Erez, and Yuval Tassa. Mujoco: A physics engine for model-based control. In *2012 IEEE/RSJ international conference on intelligent robots and systems*, pages 5026–5033. IEEE, 2012.

[38] Kyriakos G Vamvoudakis and Frank L Lewis. Online actor–critic algorithm to solve the continuous-time infinite horizon optimal control problem. *Automatica*, 46(5):878–888, 2010.

[39] Oriol Vinyals, Igor Babuschkin, Wojciech M Czarnecki, Michaël Mathieu, Andrew Dudzik, Junyoung Chung, David H Choi, Richard Powell, Timo Ewalds, Petko Georgiev, et al. Grandmaster level in starcraft ii using multi-agent reinforcement learning. *nature*, 575(7782):350–354, 2019.

[40] Brent A Wallace and Jennie Si. Continuous-time reinforcement learning control: A review of theoretical results, insights on performance, and needs for new designs. *IEEE Transactions on Neural Networks and Learning Systems*, 2023.

[41] Haoran Wang, Thaleia Zariphopoulou, and Xun Yu Zhou. Reinforcement learning in continuous time and space: A stochastic control approach. *Journal of Machine Learning Research*, 21 (198):1–34, 2020.

[42] Sifan Wang, Yujun Teng, and Paris Perdikaris. Understanding and mitigating gradient flow pathologies in physics-informed neural networks. *SIAM Journal on Scientific Computing*, 43 (5):A3055–A3081, 2021.

[43] Sifan Wang, Xinling Yu, and Paris Perdikaris. When and why pinns fail to train: A neural tangent kernel perspective. *Journal of Computational Physics*, 449:110768, 2022.

[44] Xuefeng Wang, Xinran Li, Jiawei Shao, and Jun Zhang. Ac2c: Adaptively controlled two-hop communication for multi-agent reinforcement learning. *arXiv preprint arXiv:2302.12515*, 2023.

[45] E Weinan, Jiequn Han, and Arnulf Jentzen. Algorithms for solving high dimensional pdes: from nonlinear monte carlo to machine learning. *Nonlinearity*, 35(1):278, 2021.

[46] Harley E Wiltzer, David Meger, and Marc G Bellemare. Distributional hamilton-jacobi-bellman equations for continuous-time reinforcement learning. In *International Conference on Machine Learning*, pages 23832–23856. PMLR, 2022.

[47] Yongliang Yang, Weinan Gao, Hamidreza Modares, and Cheng-Zhong Xu. Robust actor–critic learning for continuous-time nonlinear systems with unmodeled dynamics. *IEEE Transactions on Fuzzy Systems*, 30(6):2101–2112, 2021.

[48] Cagatay Yildiz, Markus Heinonen, and Harri Lähdesmäki. Continuous-time model-based reinforcement learning. In *International Conference on Machine Learning*, pages 12009–12018. PMLR, 2021.

[49] Chao Yu, Akash Velu, Eugene Vinitsky, Jiaxuan Gao, Yu Wang, Alexandre Bayen, and Yi Wu. The surprising effectiveness of ppo in cooperative multi-agent games. *Advances in neural information processing systems*, 35:24611–24624, 2022.

[50] Lei Zhang, Mukesh Ghimire, Zhe Xu, Wenlong Zhang, and Yi Ren. Pontryagin neural operator for solving general-sum differential games with parametric state constraints. In *6th Annual Learning for Dynamics & Control Conference*, pages 1728–1740. PMLR, 2024.

[51] Lei Zhang, Mukesh Ghimire, Wenlong Zhang, Zhe Xu, and Yi Ren. Value approximation for two-player general-sum differential games with state constraints. *IEEE Transactions on Robotics*, 2024.

A Mathematical Proof

A.1 Proof of Lemma 3.1

Proof. Given all $(x,t) \in \mathcal{X} \times [0,T]$ and a small horizon $\Delta t > 0$, we apply a Taylor expansion to the definition of $V(x,t)$ in Eq. (2) to derive the HJB PDE as follows:

$$
\begin{aligned}
V(x,t) &= \max_{u\in\mathcal{U}} \int_t^T e^{-\rho(\tau-t)} r(x,u) d\tau + g(x_T) \\
&= \max_{u\in\mathcal{U}} \int_t^{t+\Delta t} e^{-\rho(\tau-t)} r(x(\tau),u(\tau)) d\tau + \max_{u\in\mathcal{U}} \int_{t+\Delta t}^T e^{-\rho(\tau-t)} r(x(\tau),u(\tau)) d\tau + g(x_T) \\
&= \max_{u\in\mathcal{U}} \int_t^{t+\Delta t} e^{-\rho(\tau-t)} r(x(\tau),u(\tau)) d\tau + \max_{u\in\mathcal{U}} \int_t^{T-\Delta t} e^{-\rho(s+\Delta t-t)} r(x(s+\Delta t),u(s+\Delta t)) ds + g(x_T) \\
&= \max_{u\in\mathcal{U}} \int_t^{t+\Delta t} e^{-\rho(\tau-t)} r(x(\tau),u(\tau)) d\tau + e^{-\rho\Delta t}(\max_{u\in\mathcal{U}} \int_t^{T-\Delta t} e^{-\rho(s-t)} r(x(s+\Delta t),u(s+\Delta t)) ds + g(x_T)) \\
&\approx \max_{u\in\mathcal{U}} \int_t^{t+\Delta t} e^{-\rho(\tau-t)} r(x(\tau),u(\tau)) d\tau + e^{-\rho\Delta t}(\max_{u\in\mathcal{U}} \int_{t+\Delta t}^T e^{-\rho(\tau-t)} r(x(\tau),u(\tau)) d\tau + g(x_T)) \\
&\approx \max_{u\in\mathcal{U}} r(x,u)\Delta t + e^{-\rho\Delta t} \max_{u\in\mathcal{U}} V(x(t+\Delta t), t+\Delta t) \\
&= \max_{u\in\mathcal{U}} r(x,u)\Delta t + (1-\rho\Delta t + o(\Delta t)) \max_{u\in\mathcal{U}} (V(x,t) + \partial_t V(x,t)\Delta t + \nabla_x V(x,t)^\top f(x,u)\Delta t + o(\Delta t))
\end{aligned}
$$

By canceling out $V(x,t)$ on both sides of the above equality, we obtain that

$$-\rho V(x,t)\Delta t + \partial_t V(x,t)\Delta t + \max_{u\in\mathcal{U}} (\nabla_x V(x,t)^\top f(x,u) + r(x,u))\Delta t + o(\Delta t) = 0$$

Dividing by Δt and letting $\Delta t \to 0$, we have that

$$-\rho V(x,t) + \partial_t V(x,t) + \max_{u\in\mathcal{U}} (\nabla_x V(x,t)^\top f(x,u) + r(x,u)) = 0.$$

Therefore, the $V(x,t)$ is the optimal solution to the following HJB PDEs:

$$-\rho V(x,t) + \partial_t V(x,t) + \nabla_x V(x,t)^\top f(x,u^*) + r(x,u^*) = 0,$$

with boundary condition $V(x,T) = g(x)$.

Here optimal control input is $u^* = \arg\max_{u\in\mathcal{U}} \mathcal{H}(x,t,\nabla_x V(x,t))$, where $\mathcal{H}$ is the Hamiltonian defined as $\mathcal{H} = \nabla_x V(x,t)^\top f(x,u) + r(x,u)$. □

A.2 Proof of Lemma 3.2

Proof. Recall the one-step Q-function over a short interval $\delta t > 0$, where u is the optimal control input.

$$Q(x,t,u) = r(x,u)\,\delta t + e^{-\rho\delta t}\, V\big(x(t+\delta t),\, t+\delta t\big).$$

For small δt we have the first-order Taylor expansion in both state and time:

$$V\big(x(t+\delta t),\, t+\delta t\big) = V(x,t) + \nabla_x V(x,t)^\top f(x,u)\,\delta t + \partial_t V(x,t)\,\delta t + o(\delta t).$$

Similarly, $e^{-\rho\delta t} = 1 - \rho\,\delta t + o(\delta t)$.

Plugging both expansions into $Q(x,t,u)$ gives

$$
\begin{aligned}
Q(x,t,u) &= r(x,u)\,\delta t + \big(1-\rho\,\delta t + o(\delta t)\big)\Big[V(x,t) + \nabla_x V(x,t)^\top f(x,u)\,\delta t + \partial_t V(x,t)\,\delta t + o(\delta t)\Big] \\
&= r(x,u)\,\delta t + V(x,t) + \big[\nabla_x V(x,t)^\top f(x,u) + \partial_t V(x,t) - \rho V(x,t)\big]\delta t + o(\delta t).
\end{aligned}
$$

Subtract $V(x,t)$ and discard the higher-order term:

$$Q(x,t,u) - V(x,t) = [-\rho V(x,t) + \partial_t V(x,t) + \nabla_x V(x,t)^\top f(x,u) + r(x,u)]\delta t + o(\delta t).$$

Dividing by δt and letting $\delta t \to 0$ yields the instantaneous advantage density

$$A(x,t,u) = \lim_{\delta t\to 0} \frac{Q(x,t,u) - V(x,t)}{\delta t} = -\rho V(x,t) + \partial_t V(x,t) + \nabla_x V(x,t)^\top f(x,u) + r(x,u).$$

This completes the proof. □

A.3 Proof of Lemma 3.3

Policy Improvement via State-Action Value Function. We consider the standard policy improvement step, where the new policy is obtained by maximizing the state-action value function:

$$\pi_{\text{new}}(x,t) = \arg\max_{u\in\mathcal{U}} Q^{\pi_{\text{old}}}(x,t,u),$$

where the one-step Q-function with a small $\delta t > 0$ is defined as:

$$\begin{aligned} Q(x,t,u) &= r(x,u)\,\delta t + e^{-\rho\delta t} V\big(x(t+\delta t), t+\delta t\big) \\ &= r(x,u)\,\delta t + e^{-\rho\delta t}\mathbb{E}_{u'\sim\pi(\cdot|x')}\left[Q(x',t+\delta t,u')\right], \end{aligned}$$

Since we assume the goal state function stays invariant, we only define the $Q^\pi = \int_0^T e^{-\rho t} r_t dt$. Because the new policy π^{new} yields equal or higher value in expectation:

$$\mathbb{E}_{u\sim\pi_{\text{new}}}\left[Q^{\pi_{\text{old}}}(x,t,u)\right] \geq \mathbb{E}_{u\sim\pi_{\text{old}}}\left[Q^{\pi_{\text{old}}}(x,t,u)\right].$$

Then we can have:

$$\begin{aligned} Q^{\pi_{\text{old}}} &= r_0\,\delta t + e^{-\rho\delta t}(\mathbb{E}_{u_1\sim\pi_{\text{old}}}\left[Q^{\pi_{\text{old}}}(x_1,t_1,u_1)\right]) \\ &\leq r_0\,\delta t + e^{-\rho\delta t}\left(\mathbb{E}_{u_1\sim\pi_{\text{new}}}\left[Q^{\pi_{\text{old}}}(x_1,t_1,u_1)\right]\right) \\ &= r_0\,\delta t + e^{-\rho t_1} r_1\,\delta t + e^{-\rho\delta t}\left(\mathbb{E}_{u_2\sim\pi_{\text{old}}}\left[Q^{\pi_{\text{old}}}(x_2,t_2,u_2)\right]\right) \\ &\leq r_0\,\delta t + e^{-\rho t_1} r_1\,\delta t + e^{-\rho\delta t}\left(\mathbb{E}_{u_2\sim\pi_{\text{new}}}\left[Q^{\pi_{\text{old}}}(x_2,t_2,u_2)\right]\right) \\ &= r_0\,\delta t + e^{-\rho t_1} r_1\,\delta t + e^{-\rho t_2} r_2\,\delta t + e^{-\rho\delta t}\left(\mathbb{E}_{u_3\sim\pi_{\text{old}}}\left[Q^{\pi_{\text{old}}}(x_3,t_3,u_3)\right]\right). \\ &\vdots \\ &\leq \int_0^T e^{-\rho t} r_t dt \\ &= Q^{\pi_{\text{new}}}. \end{aligned}$$

□

A.4 Derivation of Definition 2

Proof. We consider the value function defined in Eq. (2) and follow the Proof of Lemma 3.1 to write out the dynamic programming principle of $V(x,t)$ as:

$$V(x_t,t) = r(x_t,u_t)\Delta t + e^{-\rho\Delta t} V(x_{t+\Delta t}, t+\Delta t).$$

where u is the optimal control input. Taking the gradient with respect to x on both sides using the chain rule:

$$\nabla_x V(x_t,t) = \nabla_x r(x_t,u_t)\Delta t + e^{-\rho\Delta t}\nabla_x f(x_t,u_t)^\top \nabla_x V(x_{t+\Delta t}, t+\Delta t).$$

which matches the estimator proposed in Definition 2. □

A.5 Proof of Theorem 3.4

Proof. From VGI in definition 2, with an Euler step gives $x_{t+\Delta t} = x_t + f(x_t,u_t)\Delta t + o(\Delta t)$, we have the first-order-accurate VGI approximation:

$$\nabla_x V(x_t,t) = \nabla_x r(x_t,u_t)\Delta t + e^{-\rho\Delta t}\big[I + \nabla_x f(x_t,u_t)\Delta t\big]^\top \nabla_x V(x_{t+\Delta t}, t+\Delta t).$$

Rewrite VGI approximation as the affine map $\zeta = G(\zeta)$ with

$$b = \nabla_x r(x_t,u_t)\Delta t,\ A = e^{-\rho\Delta t}\big[I + \nabla_x f(x_t,u_t)\Delta t\big]^\top,\ \zeta = \nabla_x V(\cdot,\cdot).$$

Assume the dynamics have a bounded Jacobian $\|\nabla_x f(x_t,u_t)\| \leq L_f$. Then

$$\|A\| \leq e^{-\rho\Delta t}(1 + L_f\Delta t) = \beta.$$

Because we study high-frequency settings, Δt is chosen sufficiently small, which makes $L_f\Delta t \to 0$, so that $\beta < 1$. For any $\zeta_1, \zeta_2 \in \mathbb{R}^d$,

$$\|G(\zeta_1) - G(\zeta_2)\| = \|A(\zeta_1 - \zeta_2)\| \leq \beta\|\zeta_1 - \zeta_2\|,$$

Hence, G is a contraction. Banach's fixed-point theorem guarantees a unique fixed point ζ^* and linear convergence $\|\zeta^{(k)} - \zeta^*\| \leq \beta^k\|\zeta^{(0)} - \zeta^*\|$. Therefore, the value-gradient iteration converges, completing the proof. □

A.6 Training Algorithm

We present the training algorithm for our proposed approach, Value Iteration via PINN (VIP), as follows:

Algorithm 1 Value Iteration via PINN (VIP)

Init: value net V_θ, policy nets $\{\pi_{\omega_i}\}_{i=1}^N$, dynamics $\hat{f}_\psi$, reward $\hat{r}_\phi$
for $l = 1, \ldots, T$ **do**
  ▷ **Collect one rollout:**
  $x \leftarrow \text{env.reset}()$
  for $k = 1, \ldots, K$ **do**
    sample decision time $t \sim \mathcal{T}$ ▷ t is arbitrary time
    for each agent $i = 1, \ldots, N$ **do**
      $u_i \sim \pi_{\omega_i}(u_i \mid x, t)$
    end for
    set joint action $u = (u_1, \ldots, u_N)$
    $(x', r) \leftarrow \text{env.step}(u)$
    append (x, t, u, r, x') to local rollout $\mathcal{R}$
    $x \leftarrow x'$
  end for
  ▷ **Dynamics and Reward Model learning on** $\mathcal{R}$
  update ψ, ϕ as per the Equation (14) and (15).
  ▷ **Critic update on** $\mathcal{R}$
  compute all losses $\mathcal{L}_{\text{res}}, \mathcal{L}_{\text{term}}, \mathcal{L}_{\text{anchor}}, \mathcal{L}_{\text{vgi}}$ by Equation (5), (17), (13).
  $\theta \leftarrow \theta - \alpha_V \nabla_\theta(\ldots)$
  ▷ **Actor update for each agent**
  for $i = 1, \ldots, N$ **do**
    compute $A(x, t, u)$ for all $(x, t, u) \in \mathcal{R}$
    $\omega_i \leftarrow \omega_i - \alpha_\pi \nabla_{\omega_i}\big(-\mathbb{E}_{(x,t,u)\in\mathcal{R}}[\, A(x, t, u)\, \log \pi_{\omega_i}(u_i \mid x, t)\,]\big)$ by Equation (9).
  end for
end for

B Environmental Settings

B.1 Coupled Oscillator

We evaluate on a two-agent *coupled spring–damper* system. Each agent $i \in \{1, 2\}$ controls one mass in a pair of identical oscillators with linear coupling. The continuous-time dynamics are

$$\begin{aligned} \dot{x}_i &= v_i, \\ \dot{v}_i &= -\,k\,x_i \;-\; b\,v_i \;+\; u_i, \end{aligned} \qquad i = 1, 2, \tag{19}$$

where

- x_i and v_i are the position and velocity of mass i;
- $k = 1.0$ is the spring constant, and $b = 0.5$ is the damping coefficient;
- $u_i \in [-u_{\max}, u_{\max}]$ is the control force applied by agent i, with $u_{\max} = 10$.

At each step the joint reward is

$$r = -\Big(x_1^2 + x_2^2 \;+\; \lambda_c\,(x_1 - x_2)^2 \;+\; \beta\,(u_1^2 + u_2^2)\Big),$$

with coupling strength $\lambda_c = 2.0$ and control penalty $\beta = 0.01$. We normalize by a constant factor (here $1/10$) so that $r \in [-1, 0]$.

For the coupled oscillator with linear dynamics

$$\dot{x} = A\,x + B\,u,$$

we can compute the exact infinite-horizon LQR solution:

1. Solve the continuous algebraic Riccati equation (CARE)

$$A^\top P + P\,A - P\,B\,R^{-1}B^\top P + Q = 0$$

for the symmetric matrix $P \in \mathcal{R}^{4\times 4}$.

2. Form the optimal state-feedback gain

$$K \;=\; R^{-1}B^\top P.$$

3. The optimal control law is

$$u^*(x) \;=\; -\,K\,x, \qquad u_i^* = -K_i\,x,$$

where K_i is the i-th row of K.

4. The corresponding optimal value function is the quadratic form

$$V^*(x) \;=\; x^\top P\,x,$$

whose exact gradient is

$$\nabla_x V^*(x) \;=\; 2\,P\,x.$$

We use $u^*(x)$, $V^*(x)$, and $\nabla_x V^*(x)$ as ground truth targets when evaluating the precision of the policy, the error of the value function, and the consistency of the gradient.

B.2 Continuous-Time MPE

We build on the standard MPE of [25], which simulates N holonomic agents in a 2D world with simple pairwise interactions. In the original MPE each control step advances the physics by a fixed time-step $\Delta t_{\text{fixed}} = 0.1\,\text{s}$. To evaluate our continuous-time framework under irregular sampling, we modify the simulator so that at each step the integration interval is drawn randomly,

$$\Delta t_k \;\sim\; \text{Uniform}(\Delta t_{\min},\, \Delta t_{\max}).$$

The underlying dynamics, observation and action spaces, reward functions, and task definitions remain exactly as in the original MPE. For the cooperative predator-prey environment, we only control the predators (3 agents) action to capture the prey (1 agent). While the prey is set up with random actions.

B.3 Continuous-Time Multi-Agent MuJoCo

For high-dimensional control we adapt the discrete-time Multi-Agent MuJoCo suite (e.g. cooperative locomotion, quadruped rendezvous). By default MuJoCo uses an internal physics integrator with a base time-step of $0.01\,\text{s}$ and repeats each action for $K_{\text{fixed}} = 5$ frames, yielding an effective control interval $\Delta t_{\text{fixed}} = 0.05\,\text{s}$. We instead sample the number of frames per control step,

$$K_k \;\sim\; \text{UniformInteger}(1,\, 9),$$

so that each step advances by

$$\Delta t_k = K_k \times 0.01\ \text{s} \;\in [0.01,\, 0.09]\text{s}$$

at random. All other aspects of the environment (observations, reward structure, termination conditions) are kept identical to the original multi-agent MuJoCo tasks.

C Additional Experimental Results

Experiments were conducted on hardware comprising an Intel(R) Xeon(R) Gold 6254 CPU @ 3.10GHz and four NVIDIA A5000 GPUs. This setup ensures the computational efficiency and precision required for the demanding simulations involved in multi-agent reinforcement learning and safety evaluations.

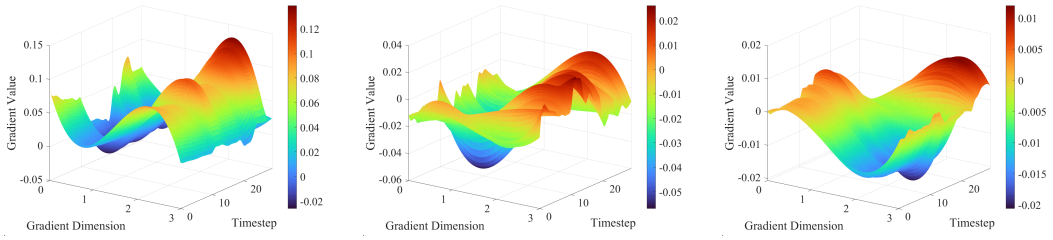

(a) Ground Truth Gradient (b) VPI Gradient w/ VGI (c) VPI Gradient w/o VGI

Figure 9: Value gradient comparison between using of VPI module.

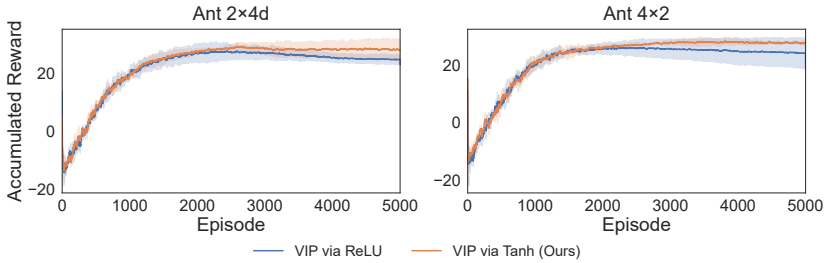

Figure 10: VIP performance with ReLU and Tanh at Ant $2 \times 4d$ and Ant 4×2.

C.1 Value Gradient Comparison

To further demonstrate the effectiveness of VIP, we sample the same trajectory in the coupled oscillator environment and compute the value gradient from the analytical LQR solution, from VIP equipped with the VGI module (ours), and from VIP trained without VGI, respectively. Fig. 9 presents the resulting 3-D surfaces. The surface in panel (b) preserves the principal ridges and valleys of the ground truth, showing that the network recovers the correct geometric structure of $\nabla_x V$; its absolute error remains below 0.02 across almost all timesteps and gradient dimensions. In contrast, the surface in panel (c) is noticeably distorted: several peaks are flattened, troughs are misplaced, and the absolute error frequently exceeds 0.08. This comparison confirms that the VIP module is critical for aligning the learned gradients with the analytical solution, thereby reducing bias and stabilising the HJB residual.

C.2 ReLU vs Tanh at Ant $2 \times 4d$ and Ant 4×2.

Fig. 10 compares VIP's learning curves when the policy network uses ReLU or Tanh activations on `Ant` $2 \times 4d$ and `Ant` 4×2. Across both tasks the Tanh implementation converges faster and attains a higher plateau reward, whereas the ReLU version peaks earlier and then undergoes a mild performance decay. The observation aligns with the earlier Tanh-versus-ReLU analysis reported in the main paper Fig. 5: smoother activation functions mitigate gradient saturation and promote more stable policy updates. The additional evidence from the two Ant variants therefore reinforces our previous claim that Tanh is better suited for value–gradient propagation in VIP.

D Hyper-parameters

As Table 1 shows, the *exploration steps* are used to delay the decay of the exploration rate: during the first 1000 steps, the exploration schedule remains fixed to encourage initial exploration. The *soft*

Table 1: Hyperparameter settings used in all experiments.

Parameter	**Value**
Episode length	50
Replay buffer size	10^4
Discount factor ρ	0.95
Soft update rate τ	0.001
Actor learning rate	0.0001
Critic learning rate	0.001
Dynamics model learning rate	0.001
Reward model learning rate	0.001
Exploration steps	1000
Model save interval	1000
Random seed	111-120

update rate τ controls the target network update in the critic and value estimation, where we adopt a target network with an exponential moving average to stabilize bootstrapped training. This technique helps suppress oscillations in value learning and leads to more accurate estimation of long-horizon returns.

Table 2: Summary of neural network architectures used in our framework.

Network	**Input Dimension**	**Architecture and Activation**
Value Network	State + Time $(d+1)$	FC(128) $\rightarrow$ FC(128) $\rightarrow$ FC(1), ReLU or Tanh
Dynamics Network	State + Joint Action + Time $(d+na+1)$	FC(128) $\rightarrow$ FC(128) $\rightarrow$ FC(d), ReLU
Reward Network	State + Joint Action + Time $(d+na+1)$	FC(128) $\rightarrow$ FC(128) $\rightarrow$ FC(1), ReLU
PolicyNet	Observation + Time + Time Interval $(o+2)$	FC(128) $\rightarrow$ FC(128) $\rightarrow$ FC(64) $\rightarrow$ FC(a), ReLU

Table 2 summarizes the architectures of the neural networks used in our VIP framework. All networks are implemented as FC layers with hidden size 128 unless otherwise specified. The value network takes the concatenation of the global state and time $(d+1)$ as input and outputs a scalar value. In our implementation, we use the **Tanh** activation function for the value network, as it provides smoother and more stable gradient propagation, which is critical for PINN-based value approximation. To validate this choice, we conducted an ablation study comparing **Tanh** and **ReLU** activations in the previous section.